Substrate self-derived porous rod-like NiS/Ni_9S_8/NF heterostructure as efficient bifunctional electrocatalyst for overall water splitting

Yixuan Li,[‡a] Peiyan Li,[‡a] Jiahui Jiang,[a] Ting Zhao,[a] Guancheng Xu,[*a] Li Zhang[*a, b]

[a] State Key Laboratory of Chemistry and Utilization of Carbon Based Energy Resources; College of Chemistry, Xinjiang University, Urumqi, 830017, Xinjiang, PR China.

[b] State Key Laboratory of Chemistry and Utilization of Carbon Based Energy Resources; College of Chemical Engineering, Xinjiang University, Urumqi, 830017, Xinjiang, PR China.

‡ These authors contributed equally to this work.

* Corresponding author

E-mail: zhangli420@xju.edu.cn (Li Zhang), xuguanchengxju@163.com (Guancheng Xu)

Chemicals

Nickel foam (NF) was provided by Changsha Lyrun Material Co., Ltd. Oxalic acid ($C_2H_2O_4 \cdot 2H_2O$) was purchased from Tianjin Zhiyuan Chemical Reagent Co., Ltd. Sulfur powder (S) was obtained from Tianjin Chemical Reagent Research Institute. Ruthenium dioxide (RuO_2) was obtained from Beijing Inokai Technology Co., Ltd. Commercial Platinum/carbon (Pt/C) was purchased from Shanghai Aladdin Reagent Co., Ltd. Nafion was purchased from Aladdin Reagent Co., Ltd. Potassium hydroxide (KOH) were obtained from Tianjin Xinpute Chemical Co., Ltd. All chemical reagents were used without further purification.

Material characterization

X-ray diffraction (XRD) was collected on a Bruker D8 advance diffractometer with monochromatized Cu Kα radiation (λ = 0.154 05 nm). Field-emission scanning electron microscopy (SEM), energy-dispersive X-ray spectroscopy (EDX) and elemental mapping were taken on Hitachi S-4800 microscope. Transmission electron microscopy (TEM) was taken on Hitachi H600 microscope. X-ray photoelectron spectroscopy (XPS) was measured on an Escalab 250 Xi system (Thermo Fisher Scientific).

Electrochemical characterization

All electrochemical tests were performed on a CHI660E electrochemical workstation (Shanghai Chenhua Instrument Co. Ltd.). A standard three-electrode system was used with the prepared NiS/Ni_9S_8/NF electrode as the working electrode (the geometric area is 0.5 cm^2), a standard Ag/AgCl electrode (saturated KCl solution) as the reference

electrode, a graphite rod as the counter electrode, and 1 M KOH solution as the electrolyte. All potentials reported were calibrated to the reversible hydrogen electrode (RHE): $E_{RHE} = E_{Ag/AgCl} + 0.198 + 0.059 \times pH$, pH = 13.6 for 1 M KOH. All electrochemical data were not *iR*-compensation. To make a reliable comparison, RuO_2 and Pt/C were loaded on NF with the same loading as that of NiS/Ni_9S_8/NF based catalysts. OER and HER polarization curves were recorded at a scan rates of 1 and 5 mV s^{-1}, respectively. Tafel slopes were calculated based on polarization curves. As for overall water splitting, the prepared NiS/Ni_9S_8/NF electrode were directly used as cathode and anode in a two-electrode configuration in 1.0 M KOH at room temperature. The electrochemical double-layer capacitance (C_{dl}) of the samples were measured via a simple cyclic voltammetry (CV) method to indicate the electrochemically active surface areas (ECSA). The electrochemical impedance spectroscopy (EIS) measurements were recorded with a frequency range from 0.01 kHz to 100 Hz. The long-term electrochemical stability was performed using constant voltage measurements of 10 mA cm^{-2} for all relevant reactions: HER, OER, and overall water splitting. The testing potential of chronoamperometry of HER, OER and water electrolysis is -1.05 V, 0.40 V and 1.52 V. The testing potential of Nyquist plots of HER and OER is -1.10 V and 0.42V.

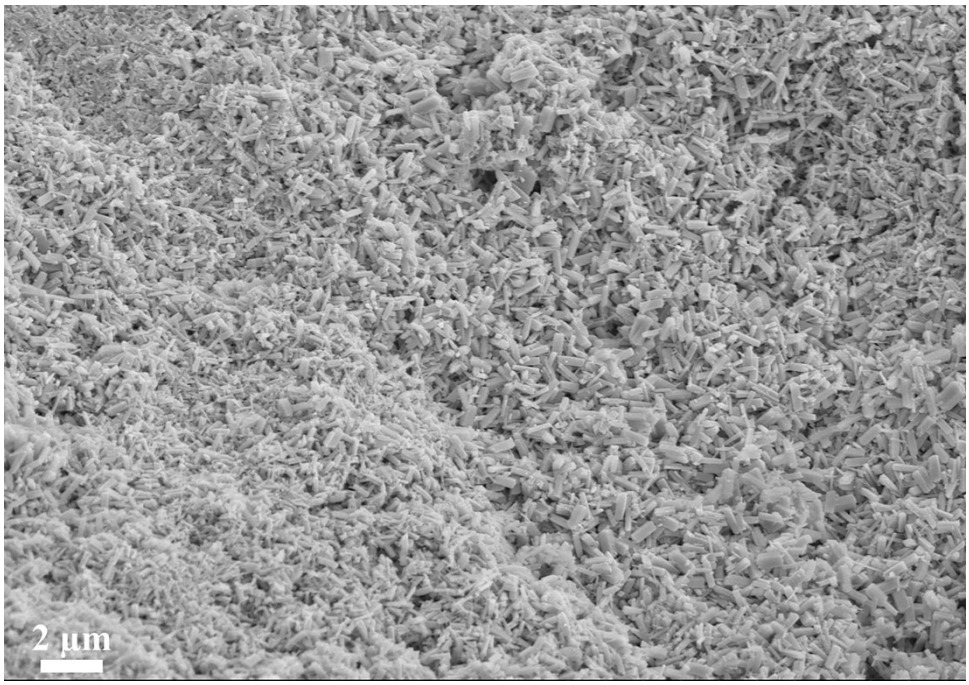

Figure S1. SEM image of $NiC_2O_4 \cdot 2H_2O$/NF-2 precursor.

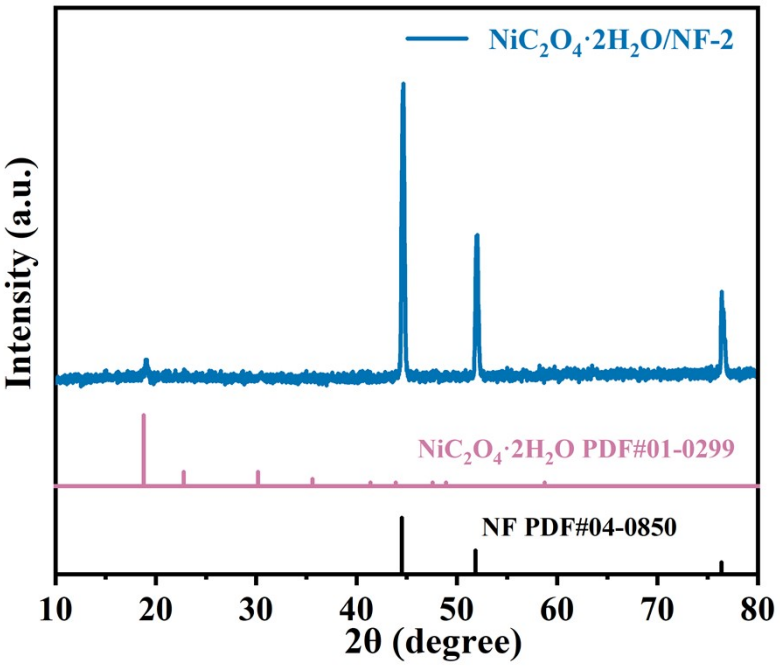

Figure S2. XRD pattern of $NiC_2O_4 \cdot 2H_2O$/NF-2 precursor.

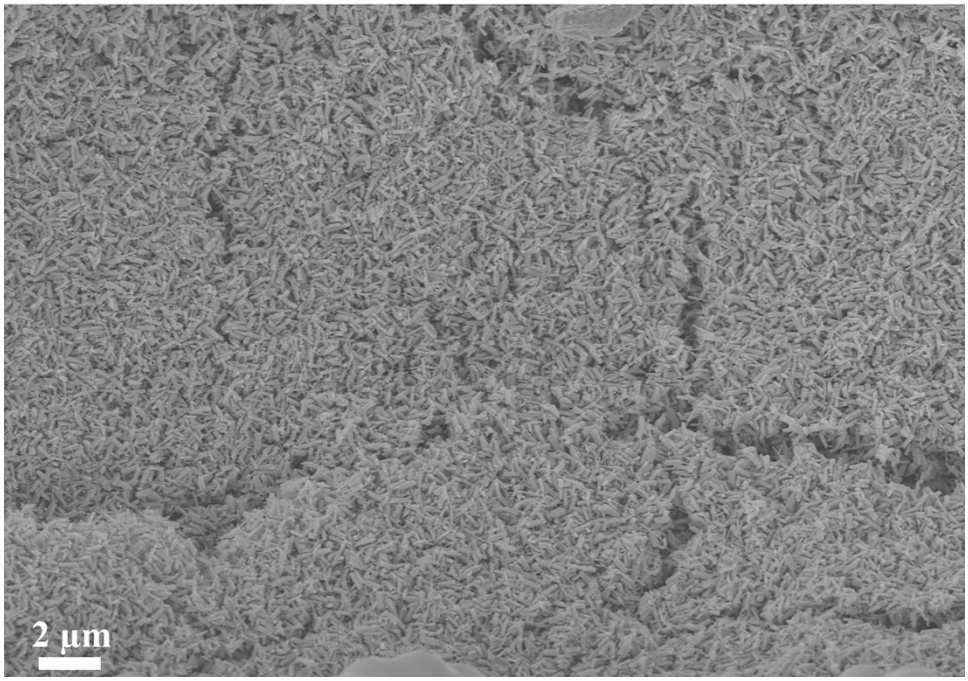

Figure S3. SEM image of NiS/Ni_9S_8/NF-2.

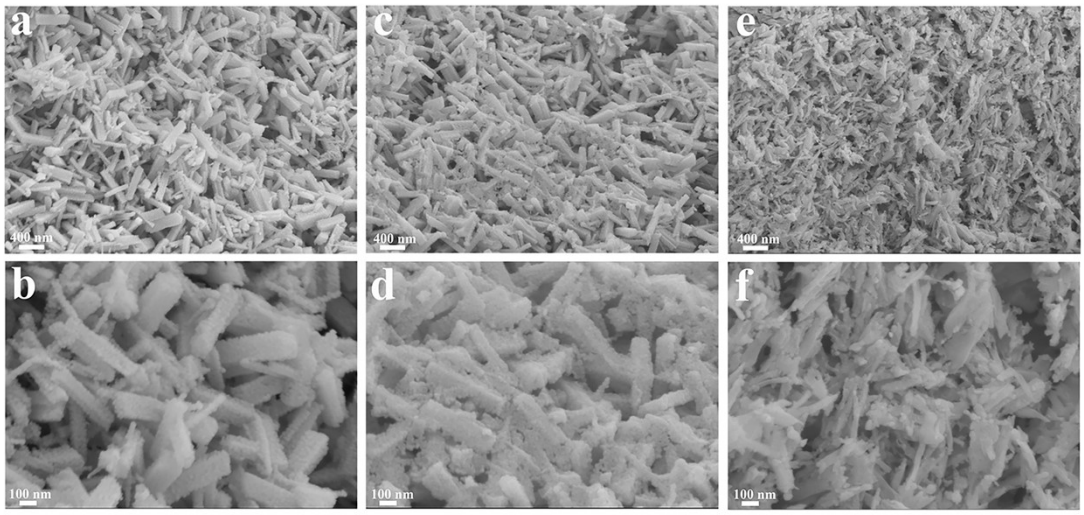

Figure S4. SEM images of (a, b) NiS/Ni_9S_8/NF-1, (c, d) NiS/Ni_9S_8/NF-3 and (e, f) NiS/Ni_9S_8/NF-4.

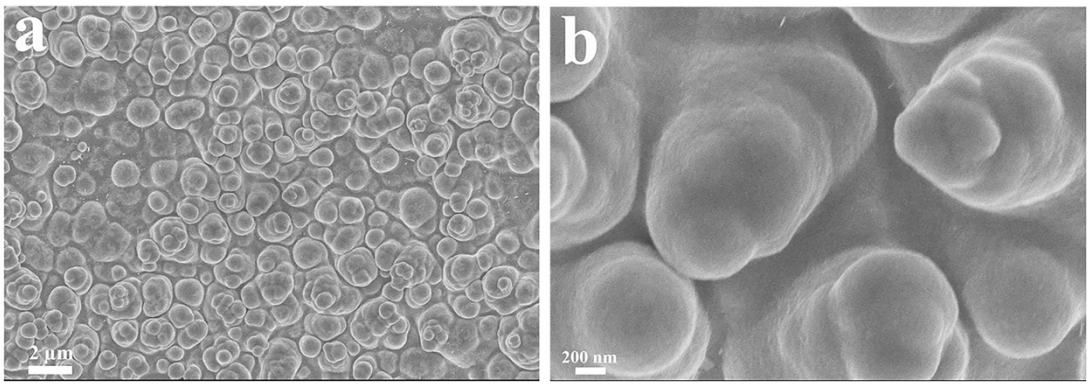

Figure S5. SEM images (a, b) of $NiS/NiS_2/Ni_3S_2/NF$.

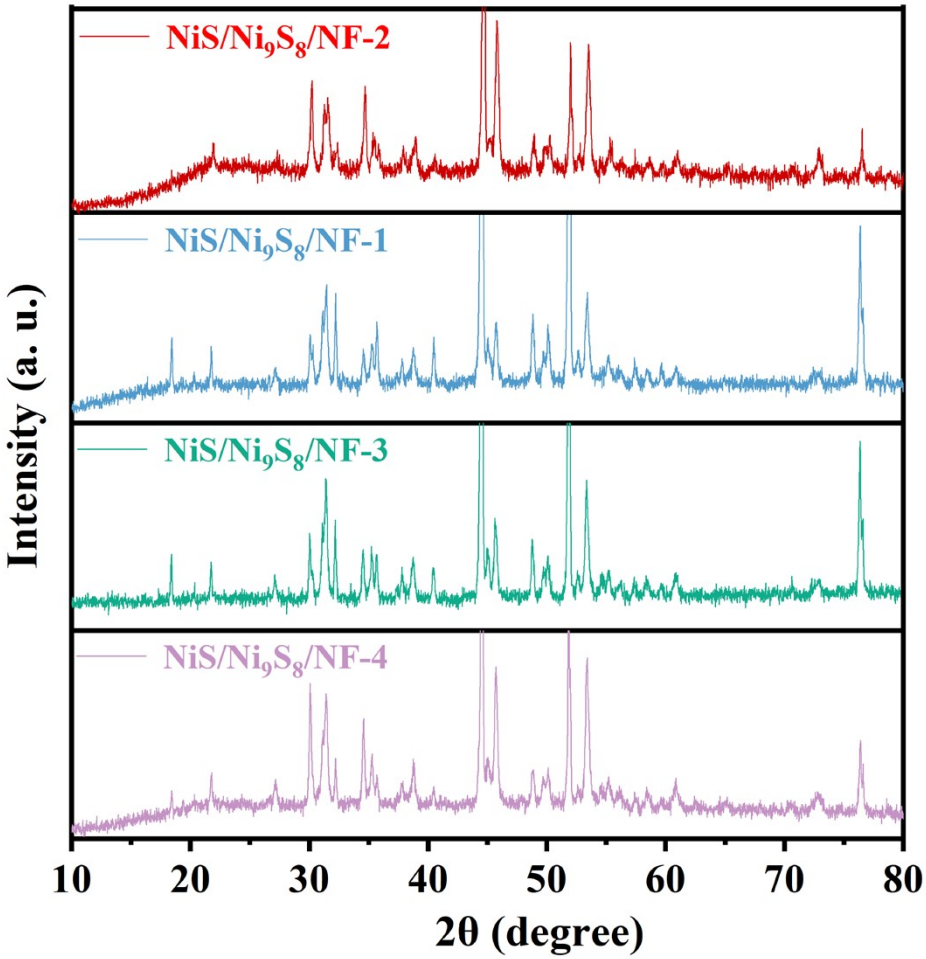

Figure S6. XRD patterns of NiS/Ni_9S_8/NF-2, NiS/Ni_9S_8/NF-1, NiS/Ni_9S_8/NF-3 and NiS/Ni_9S_8/NF-4.

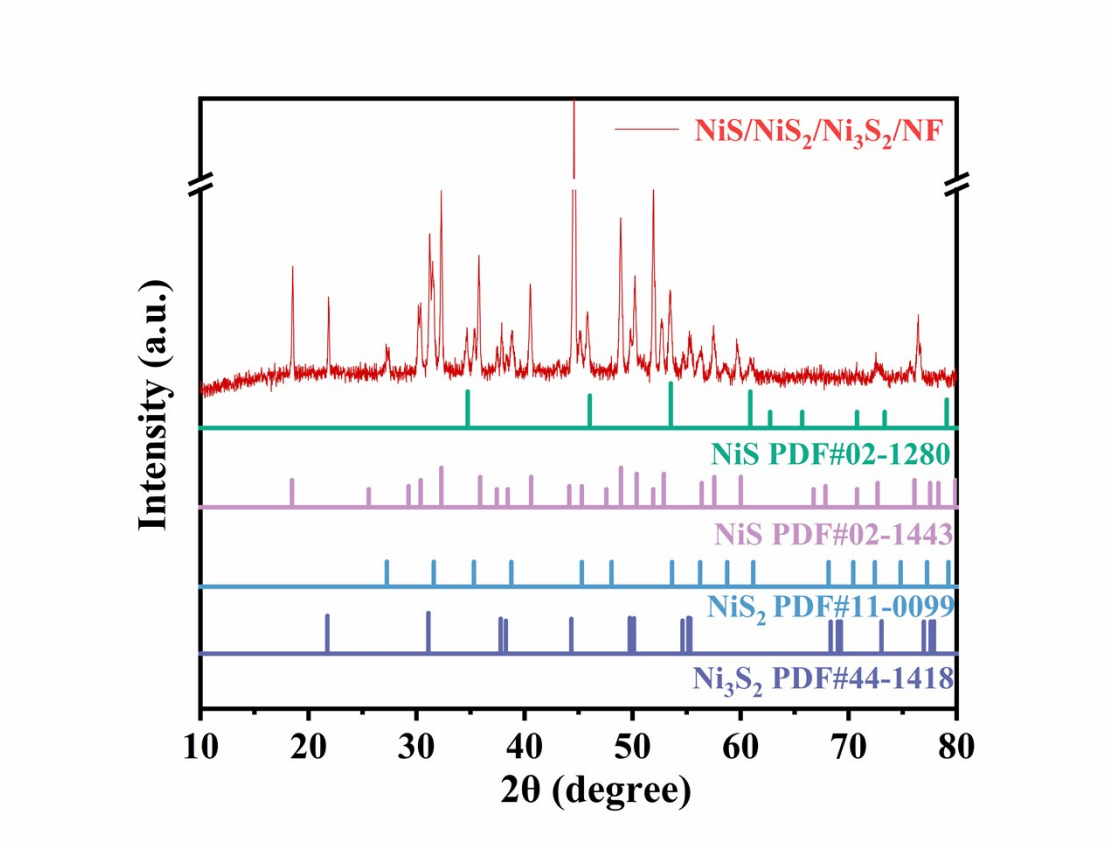

Figure S7. XRD pattern of $NiS/NiS_2/Ni_3S_2/NF$.

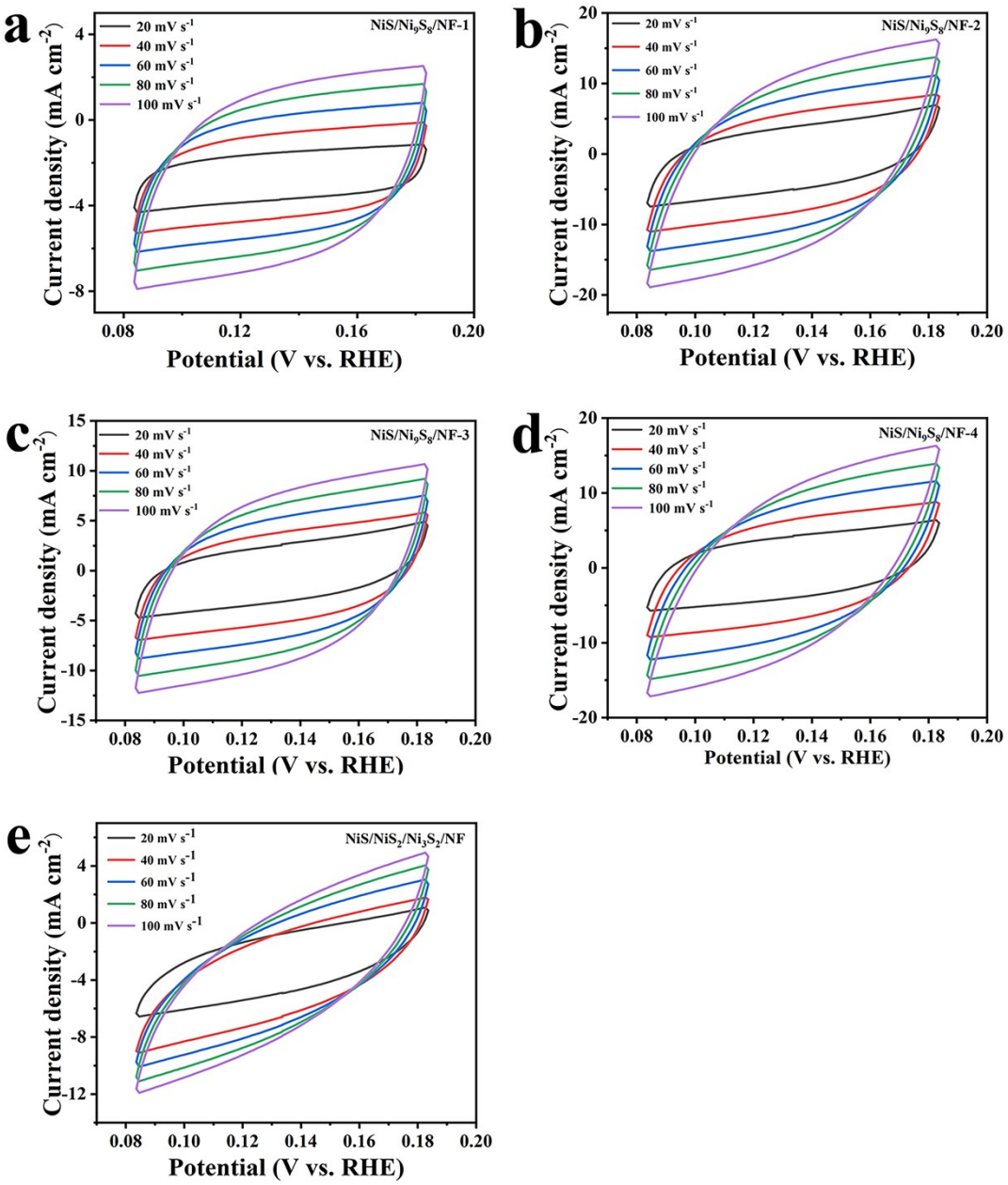

Figure S8. Cyclic voltammograms of (a) NiS/Ni_9S_8/NF-1, (b) NiS/Ni_9S_8/NF-2, (c) NiS/Ni_9S_8/NF-3, (d) NiS/Ni_9S_8/NF-4 and (e) NiS/NiS_2/Ni_3S_2/NF in -0.9 ~ -0.8 V *vs.* RHE at different scan rates from 20 mV s^{-1} to 100 mV s^{-1} in 1.0 M KOH.

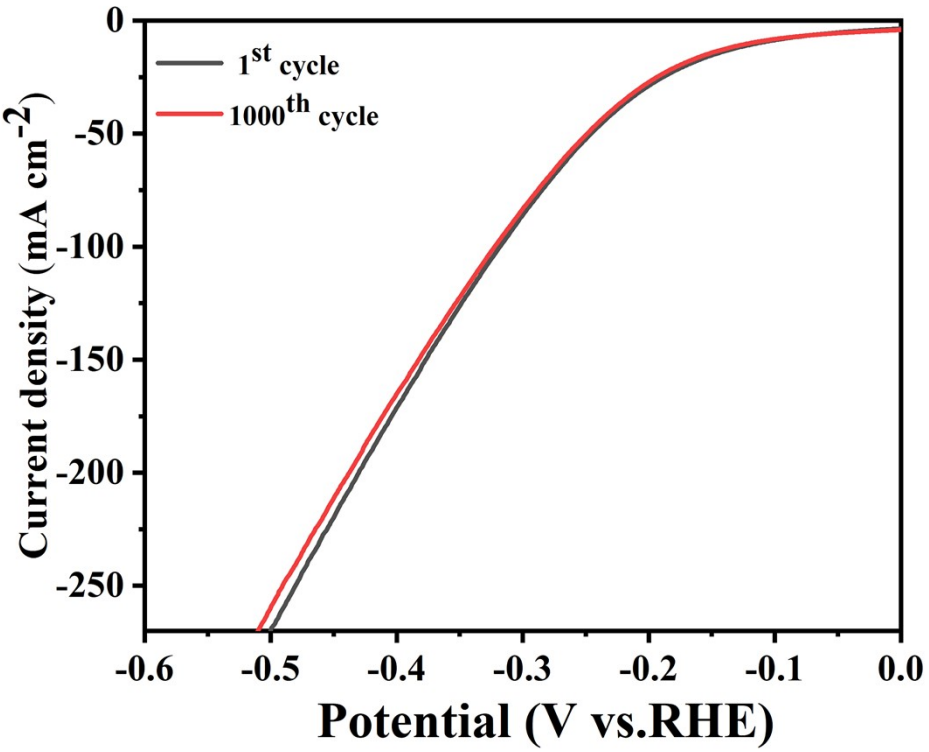

Figure S9. Polarization curves of NiS/Ni_9S_8/NF-2 before and after 1000 CV cycles.

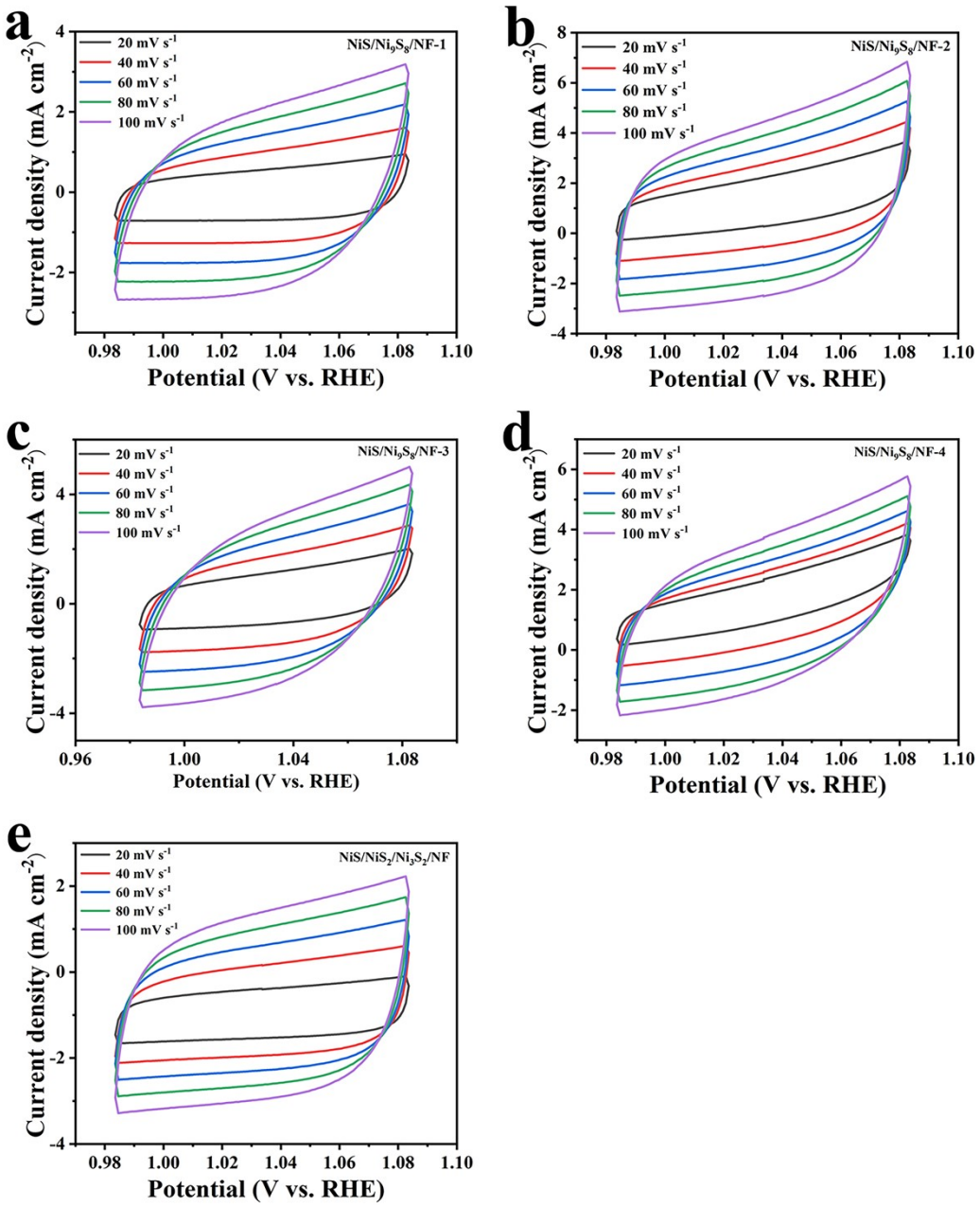

Figure S10. Cyclic voltammograms of (a) NiS/Ni_9S_8/NF-1, (b) NiS/Ni_9S_8/NF-2, (c) NiS/Ni_9S_8/NF-3, (d) NiS/Ni_9S_8/NF-4 and (e) NiS/NiS_2/Ni_3S_2/NF in -0.9 ~ -0.8 V *vs.* RHE at different scan rates from 20 mV s^{-1} to 100 mV s^{-1} in 1.0 M KOH.

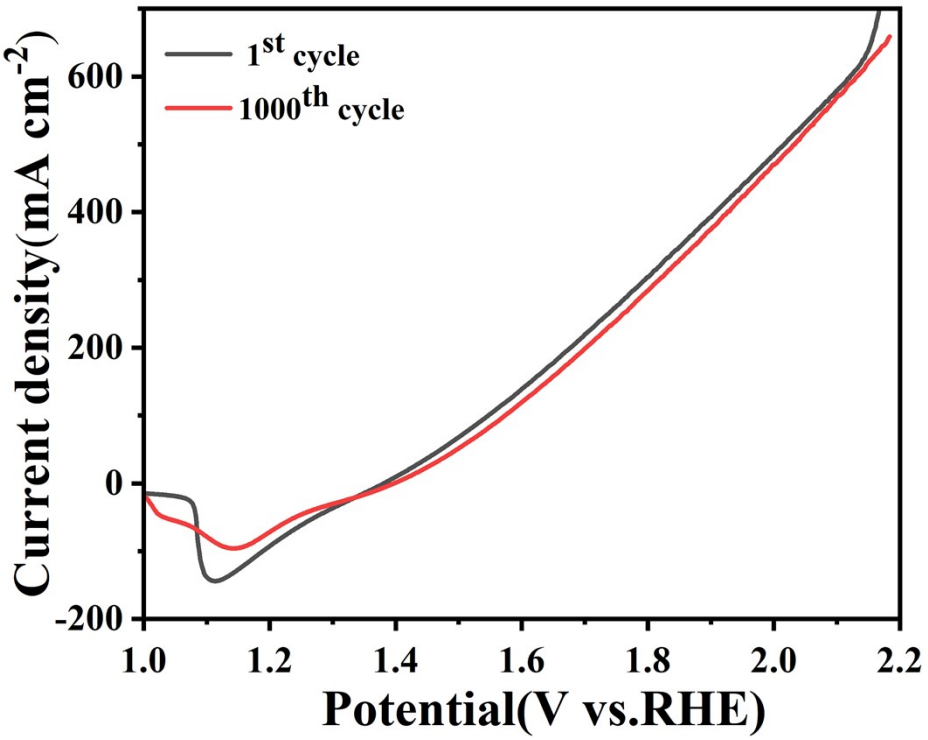

Figure S11. Polarization curves of NiS/Ni_9S_8/NF-2 before and after 1000 CV cycles.

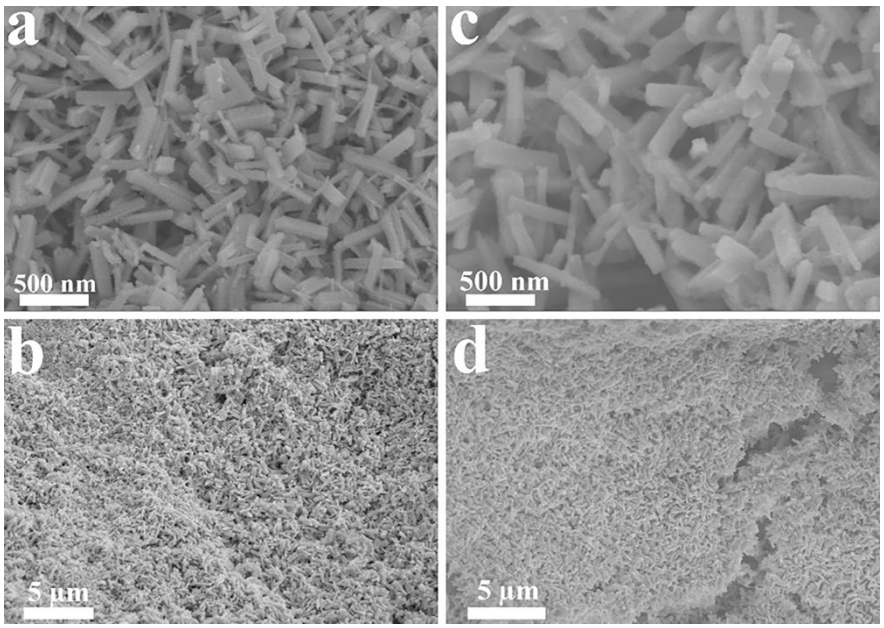

Figure S12. The SEM images of NiS/Ni_9S_8/NF-2 sample after (a,b) HER and (c,d) OER.

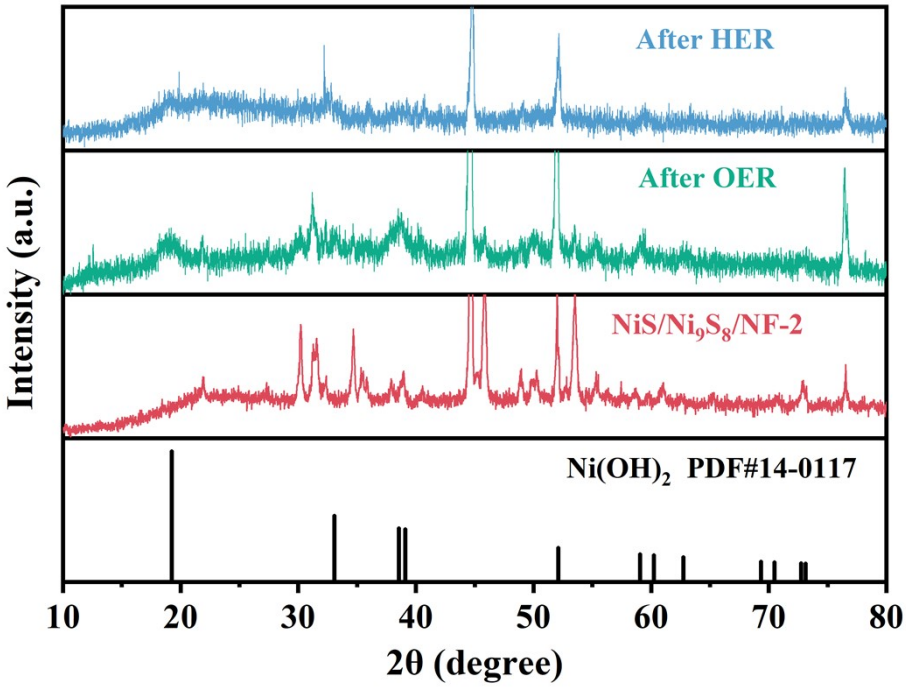

Figure S13. XRD patterns of NiS/Ni_9S_8/NF-2 after 100 h long term electrolysis for the HER and 80 h long term electrolysis for the OER.

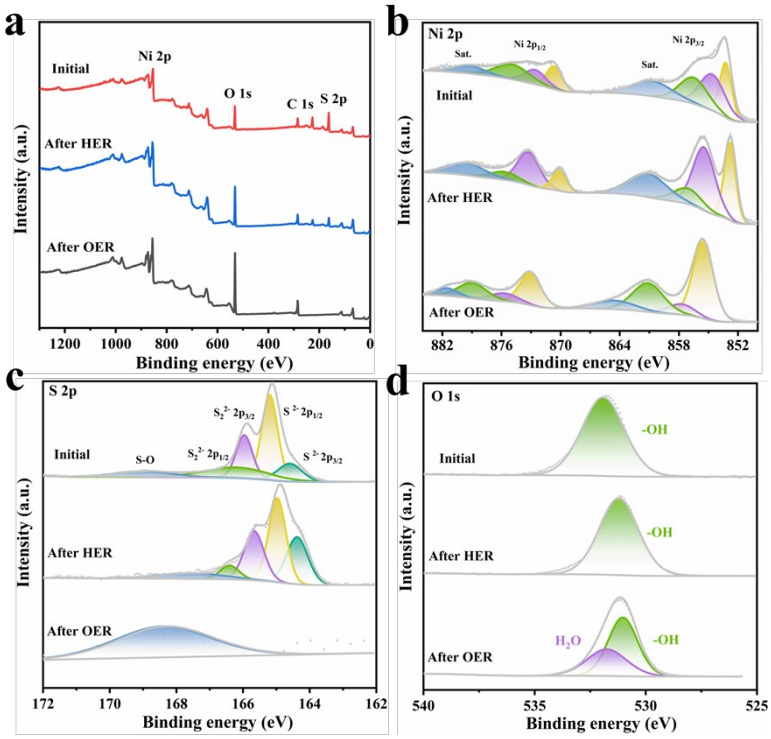

Figure S14. (a) XPS survey, (b)Ni 2p, (c)S 2p, (d) O 1s spectra of NiS/Ni_9S_8/NF-2 after i-t performance test of water splitting.

Table S1. Comparison of HER and OER activities of NiS/Ni_9S_8/NF-2 with other reported TMSs electrocatalysts

Catalyst	J ($mA\ cm^{-2}$)	Overpotential (mV)		Electrolyte	Reference
		HER	OER		
NiS/Ni_9S_8/NF-2	10	115	176	1 M KOH	**This Work**
Co_3S_4@MoS_2	10	136	280	1 M KOH	[1]
Co_3S_4@FNC-Co3	10	140	250	1 M KOH	[2]
T(Ni_3S_2/MnS-O)	10	116	228	1 M KOH	[3]
FNHNs	10	140	290	1 M KOH	[4]
$Fe_{0.8}Ni_{0.15}S_{1.05}$	10	263	228	1 M KOH	[5]
H-Fe-CoMoS	10	137	282	1 M KOH	[6]
NiS	10	-	320	1 M KOH	[7]
Fe-Ni_3S_2/FeNi	10	-	282	1 M KOH	[8]
$FeNiS_2$ NS/rGO	10	-	200	1 M KOH	[9]
CoNi-S/NS-rGO-550	10	-	290	1 M KOH	[10]
NiCoFe-PS	10	-	195	1 M KOH	[11]
Ni_3S_2	10	-	256	1 M KOH	[12]
N-CoS_2@graphene	10	-	205	1 M KOH	[13]
Fe-MoS/carbon nanocomposites	10	321	-	1 M KOH	[14]
a-CoSx	10	182	-	1 M KOH	[15]
CoS@NiCoLDH	10	124	-	1 M KOH	[16]

Table S2. Comparison of overall water splitting activities of NiS/Ni_9S_8/NF-2 with other reported TMSs electrocatalysts

Catalysts (Cathode)	Catalysts (anode)	J ($mA\ cm^{-2}$)	Potential (V)	Reference
NiS/Ni_9S_8/NF-2	**NiS/Ni_9S_8/NF-2**	10	1.53	**This Work**
Co_3S_4@MoS_2	**Co_3S_4@MoS_2**	10	1.58	[1]
Co_3S_4@FNC-Co3	**Co_3S_4@FNC-Co3**	10	1.58	[2]
T(Ni_3S_2/MnS-O)	**T(Ni_3S_2/MnS-O)**	10	1.54	[3]
FNHNs	**FNHNs**	10	1.55	[4]
$Fe_{0.8}Ni_{0.15}S_{1.05}$	**$Fe_{0.8}Ni_{0.15}S_{1.05}$**	10	1.63	[5]
V-NiS_2	**V-NiS_2**	10	1.56	[17]
S, N-CNTs/ CoS_2@Co	**S,NCNTs/CoS_2@Co**	10	1.63	[18]
Ni_3S_2-FeS	**Ni_3S_2-FeS**	10	1.61	[19]
$CoNi_2S_4$	**$CoNi_2S_4$**	10	1.58	[20]
SW-CoS@CNT	**SW-CoS@CNT**	10	1.56	[21]

References

[1] Y. Guo, J. Tang, Z. Wang, Y. M. Kang, Y. Bando, Y. Yamauchi, *Nano Energy*, 2018, **47**, 494-502.

[2] L. Han, Y. Wu, B. Zhao, W. Meng, D. Zhang, M. Li, R. Pang, Y. Zhang, A. Cao, Y. Shang, *ACS Appl. Mater. Interfaces*, 2022, **14**, 30847-30856.

[3] X. Zhu, J. Dai, L. Li, D. Zhao, Z. Wu, Z. Tang, L.-J. Ma, S. Chen, *Carbon*, 2020 **160**, 133-144.

[4] Y. Zhang, J. Fu, H. Zhao, R. Jiang, F. Tian, R. Zhang, *Appl. Catal. B-Environ.*, 2019, **257**, 117899.

[5] J. Liu, Y. Yang, B. Ni, H. Li, X. Wang, *Small*, 2017, **13**, 1602637,

[6] Z. Jing, Q. Zhao, D. Zheng, L. Sun, J. Geng, Q. Zhou, J. Lin, *J. Mater. Chem. A*, 2020, **8**, 20323-20330.

[7] Y. Guo, X. Zhou, J. Tang, S. Tanaka, Y. V. Kaneti, J. Na, B. Jiang, Y. Yamauchi, Y. Bando, Y. Sugahara, *Nano Energy*, 2020, **75**, 104913.

[8] O. Mabayoje, A. Shoola, B. R. Wygant, C.B. Mullins, *ACS Energy Lett.*, 2016, **1**, 195-201.

[9] C. Z. Yuan, Z. T. Sun, Y. F. Jiang, Z. K. Yang, N. Jiang, Z. W. Zhao, U. Y. Qazi, W. H. Zhang, A. W. Xu, *Small*, 2017, **13**, 1604161.

[10] J. Jiang, S. Lu, W. K. Wang, G. X. Huang, B. C. Huang, F. Zhang, Y. J. Zhang, H. Q. Yu, *Nano Energy*, 2018, **43**, 300-309.

[11] M. B. Zakaria, D. Zheng, U. P. Apfel, T. Nagata, E. S. Kenawy, J. Lin, *ACS Appl. Mater. Interfaces*, 2020, **12**, 40186-40193.

[12] M. Yao, H. Hu, B. Sun, N. Wang, W. Hu, S. Komarneni, *Small*, 2019, **15**, e1905201.

[13] M. Lee, H. S. Oh, M. K. Cho, J. P. Ahn, Y. J. Hwang, B. K. Min, *Appl. Catal. B-Environ.*, 2018, **233**, 130-135.

[14] W. Zhang, W. Chen, Q. Xiao, L. Yu, C. Huang, G. Lu, A.W. Morawski, Y. Yu, *Appl. Catal. B-Environ.*, 2020, **268**, 118449.

[15] Z. Huang, Z. Yang, M.Z. Hussain, Q. Jia, Y. Zhu, Y. Xia, *J. Mater. Sci. Technol.*,

2021, **84**, 76-85.

[16] W. He, R. Ifraemov, A. Raslin, I. Hod, *Adv. Funct. Mater.*, 2018, **28**, 1707244.

[17] K. Ao, Q. Wei, W.A. Daoud, *ACS Appl. Mater. Interfaces*, 2020, **12**, 33595-33602.

[18] H. Liu, Q. He, H. Jiang, Y. Lin, Y. Zhang, M. Habib, S. Chen, L. Song, *ACS Nano*, 2017, **11**, 11574-11583.

[19] J. Y. Wang, T. Ouyang, N. Li, T. Ma, Z.Q. Liu, S, *Sci. Bull.*, 2018, **63**, 1130-1140.

[20] K. Xiao, J.-X. Wei, W. K. Han, Z. Q. Liu, *J. Power Sources*, 2021, **487**, 229408.

[21] R. Zahra, E. Pervaiz, M. M. Baig, O. Rabi, *Electrochim. Acta*, 2022, **418**, 140346.